Rosaniline Hydrochloride Encapsulated MCM-48: Fluorescent and Electrochemical Sensor for Dopamine

Sarojmoni Kalita
Gauhati University
Diganta Kumar Das (digkdas@yahoo.com)
Gauhati University https://orcid.org/0000-0001-5507-016X

Research Article

Keywords: Rosaniline hydrochloride, MCM-48, Dopamine, Fluorescence, Voltammetry

Posted Date: September 21st, 2021

DOI: https://doi.org/10.21203/rs.3.rs-891347/v1

Version of Record: A version of this preprint was published at Journal of Fluorescence on October 28th, 2021. See the published version at https://doi.org/10.1007/s10895-021-02840-y.

Abstract

The dye Rosaniline hydrochloride (RANH) has been successfully incorporated in MCM-48 (designated as RANH@MCM-48) and characterised by various spectroscopic methods including FT-IR, SEM, EDX and N_2 adsorption-desorption isotherm. RANH@MCM-48 in aqueous medium acts as fluorescence “on” sensor for neurotransmitter dopamine (DA) in presence of its main biological interfering agents ascorbic acid or vitamin c (AA) along with Glucose, Cholesterol and Uric acid. The limits of detection (LOD) were found to be 65 nM and 51 nM respectively in absence and in presence of AA. The binding of DA to RANH@MCM-48 is found to be reversible with respect to $EDTA^{2-}$. The fluorescence intensity *vs.* pH plot shows a narrow fluorescence window of 7.2 to 8.8. RANH@MCM-48 has been successfully applied for DA detection in artificial cerebrospinal fluid (ACF) and bovine serum albumin (BSA) with LOD values 27 nM and 22.5 nM respectively. Platinum disc electrode has been modified with RANH@MCM-48 which showed distinct oxidation peaks with a separation of 0.188 V in cyclic voltammetry (CV). The LOD for DA in presence of AA determined from oxidation current is 77.5 nM. The voltammetric detection of DA is found to be free from common interfering species Na^+, K^+, Ca^{2+}, Fe^{2+}, Uric acid, Cholesterol and Glucose.

Introduction

Dopamine (DA) is a widely studied neurotransmitter belonging to catecholamine family which plays essential roles in the functioning of central nervous system, cardiovascular system, hormonal system, human behavioural responses such as mood, emotion, memory, and addiction [1-3]. Abnormally high levels of DA may cause Huntington’s disease [4] whereas insufficient secretion may lead to Parkinson’s disease [5] and Schizophrenia [6] which ultimately causes muscle rigidity, loss of balance, anxiety, restlessness, depression etc. Regarding the importance of DA detection and to quantify its concentration, numerous techniques such as colorimetry [7], chromatography [8], chemiluminescence [9], electrochemistry [10], capillary electrophoresis [11], UV-Vis spectroscopy [12], flow-injection analysis [13] and fluorescence spectroscopy [14] have been developed. A major concern in the electrochemical detection of DA is its coexistence with ascorbic acid (AA), the level of which is 100-1000 times higher than that of DA in biological media. Owing to their similar redox potential, selective and sensitive detection of DA is interfered by AA [15]. Therefore development of facile, sensitive, selective, cost effective and quantitative methods such as fluorescent sensors and surface modified electrodes are in high demand for the efficient detection of DA in presence of other biomolecules such as ascorbic acid, uric acid.

Nanostructured materials are emerging as efficient tool for analytical applications. Among nanostructured composites, the three dimensional cubic mesoporous silica MCM-48 described by *Ia3d* space group has notable advantages for use in detection systems [16]. They have a high surface area, high thermal stability, tunable pore size, large pore volume [17, 18] and superior to MCM-41 due to its three dimensional pore system which renders MCM-48 resistance to pore blockage and a more efficient diffusion pathway [19]. Due to these outstanding properties, they are capable of incorporating various substances like electrochemically active dyes, organic and inorganic guest molecules, active

pharmaceutical ingredients. Mesoporous silica find wide range applications in drug delivery systems [20-22], gene delivery [23], catalysis [24, 25], adsorption [26, 27], sorption and separation [28, 29], detection of heavy metals [30, 31] and biological molecules [32,34].

Dyes have been used as chemo sensors and optical sensors due to their sensitivity towards the environment and strong chromogenic ability [35]. They can be used in designing sensors by introducing them into the pores of mesoporous materials [36]. Haloi et al reported 2,7-dichlorofluorescein encapsulated Na-MMT clay as UV/Visible, fluorescence and electrochemical sensor for DA and AA [37].

In recent studies, chitosan@MCM-48 and β-cyclodextrin@MCM-48 composites were developed as bio-adsorbents for Cd^{2+} from water [38]. Another chitosan@MCM-48 nanocomposite was developed as adsorbent for removing phenol from aqueous waste water [39]. A new study has been reported for metal ion sensing via anchoring an azo dye namely 4-(4-nitro-phenylazo)-naphthalen-1-ol (NPAN) into hexagonal SBA-15, cubic SBA-16 and spherical MCM-41 [40]. Anchoring of another azo dye 1-(2-pyridylazo)-2-naphthol (PAN) into functionalised MCM-48 has also been reported for trace determination of copper, cadmium, lead and nickel in water and sea food samples [41]. Zablocka et al. developed gold electrode modified with polypyrrole-MCM-48 film for electrochemical detection of DA [42].

In this paper, we report that Rosaniline Hydrochloride dye encapsulated in MCM-48 (RAN@MCM-48) acts as a fluorescent sensor for the neurotransmitter dopamine in presence of biomolecules which commonly coexists with dopamine in biological fluids. Platinum disc electrode modified with RAN@MCM-48 leads to a significant difference in oxidation potential of dopamine and ascorbic acid in their mixture. The sensor has been successfully applied for dopamine detection in artificial cerebrospinal fluid and bovine serum albumin. The limits of detection for dopamine in different mediums are also reported.

Experimental

Materials

MCM-48, Rosaniline hydrochloride (RANH), Dopamine (DA), Ascorbic acid (AA), other biomolecules and all other chemicals were purchased either from Sigma Aldrich or LOBA. The chemicals were of analytical grade and used without further purification. The chemical solutions (10^{-3} M) were prepared in de-ionised water obtained from quartz double distilled plant. The FT-IR spectra were recorded in a Perkin Elmer RXI spectrometer as KBr pellets. The fluorescence and UV-Visible spectra were recorded in HITACHI 2500 and Shimadzu UV 1800 spectrophotometer respectively using quartz cuvette (1 cm path length). The electrochemical measurements were carried out on a CHI660DCH Instrument electrochemical analyser (USA) consisting of a three-electrode system: Pt electrode as the working electrode, Ag/AgCl (3 M NaCl) as the auxiliary electrode, Pt wire as the reference electrode and 0.1M $NaNO_3$ as supporting electrolyte. Scanning Electron Microscopy was done using Zeiss FESEM Sigma 300 and Energy Dispersive X-ray Spectroscopy was studied using Ametek EDAX. Powder X-ray diffraction (PXRD) patterns of the synthesized samples were recorded using a Rigaku Ultima IV X-Ray diffractometer (Cu K_α radiation,

λ=1.5418 Å) at 40 kV and 40 mA. The N_2 adsorption-desorption isotherm of the synthesized samples were recorded at 77 K by using Micromeritics Tristar 3000 analyser. The samples were degassed at 110 °C for 4 h prior to the measurement.

Synthesis of the sensor (RANH@MCM-48)

The sensor RANH@MCM-48 was prepared as follows: 1.0 g of MCM-48 was suspended in 20 mL deionised water and stirred for 30 minutes. To the solution, 0.25 g Rosaniline Hydrochloride (RANH) dye was added with continuous stirring for 36 hours. The solid obtained was centrifuged, washed with deionised water and the maroon solid was dried in an oven for 150°C for 12 hours to yield the dye-MCM-48 composite (RANH@MCM-48).

Synthesis of Artificial Cerebrospinal Fluid (ACF)

The ACF which contains the majority of interferents in the real cerebrospinal fluid was prepared by the reported method [43]. Briefly: 2.1 g NaCl, 0.07 g KCl, 0.08 g $CaCl_2$, 0.2 g Glucose, 0.4 g $NaHCO_3$ and 0.002 g Urea were taken and mixed together in a 250 mL volumetric flask maintaining the pH at 7.41 using phosphate buffer solution (PBS). The solution was immediately used to avoid hydrolysis of urea.

Preparation of modified electrodes (RANH@MCM-48/Pt):

10 mg of RANH@MCM-48 was dispersed in 1 mL of acetonitrile and 0.3 mL styrene. 1 µL of the solution was placed on the tip of pre cleaned platinum (Pt) electrode with the help of a micropipette and the electrodes were allowed to dry and used for further investigations. The electrode is cleaned as per reported method [44].

Results And Discussion

Characterisation of RANH@MCM-48

Thecharacterisations of RANH@MCM-48 was done by the approaches of FTIR, PXRD, N_2 adsorption-desoprtion studies and SEM-EDX analysis. The FTIR spectra of MCM-48 and RANH@MCM-48 (Fig. 1) shows a broad band at 3452 cm^{-1} and a weak band at 1638 cm^{-1} due to O-H stretching vibration and O-H bending vibration assigned to adsorbed water molecules in these materials. One broad band observed at 1093 cm^{-1} and a shoulder, observed at around 1250 cm^{-1} are due to internal and external asymmetric Si-O-Si stretching vibration respectively. The bands observed at 800 cm^{-1} and 968 cm^{-1} are assigned to symmetric stretching of Si-O-Si bonds and stretching vibration of Si-OH bonds respectively. The band observed at 1598 cm^{-1} is due to the NH_2 bond of the dye molecule. The FTIR spectra of RANH@MCM-48 also showed a series of bands in the region 1300-1590 cm^{-1} which are due to the presence of the guest molecule in the silica network.

The low angle XRD data (Fig. 2) shows a peak at 2.5^o and around 3^o corresponding to (211) and (220) plane. Two low intensity peaks appear between 4^o and 5^o corresponding to (420) and (332) plane. The pattern clearly shows presence of an Ia3d cubic mesoporous framework. The XRD pattern of RANH@MCM-48 shows a similar pattern with a decrease in intensity of the corresponding planes. The decrement in intensity indicates lossof crystallinity and ordering of the mesoporous material after introduction of dye molecule into it.

The N_2 adsorption-desorption isotherm showed typical type IV isotherm with H3 hysteresis loop which are characteristics of highly ordered mesoporous materials (Fig. 3). A sharp inflection at relative pressure p/p_o = 0.2-0.3 was observed, indicating the capillary condensation of N_2 gas within the uniform pores of MCM-48 material. The uniformity of pore size distribution was indicated by the sharpness and height of inflection point. After the introduction of the dye into the channels of cubic mesoporous MCM-48, the surface area, pore volume and pore diameter were found to decrease as evident from table 1. This suggests the occupation of pores by the dye molecules which results in the decrease of mesoporous ordering.

Table 1: Textural properties of MCM-48 and RANH@MCM-48

Material	Surface Area, A_{BET} (m^2g^{-1})	Pore Volume, V_{BJH} (cm^3g^{-1})	Pore Diameter, D_{BJH} (nm)
MCM-48	1205.03	0.48	2.52
RANH@MCM-48	567.23	0.27	2.29

Fig. 4 a showsthe SEM image of MCM-48 which have spherical morphology. After the introduction of the dye molecule, the morphology showed some distortion and irregularity of spherical shapes with agglomeration (Fig. 4 b). This indicates that the dye is deposited onto the surface and into the mesopores of MCM-48. The energy disperse X- ray analysis (EDX) confirms the coating of RAN in the pores of MCM-48 sample (Fig. 4 c, d). The energy disperses X- ray (EDX) elemental mapping analysis also demonstrates the uniform distribution of the dye into the MCM-48 material. Fig. 5 shows EDX elemental mapping of O, Si, C and N in RANH@MCM-48.

RANH@MCM-48 as Fluorescent Sensor for DA

0.01g of RANH@MCM-48 composite was dispersed in 5.0 mL of methanol and sonicated for 10 minutes to obtain a fine dispersion. 10^{-3} M DA solution was prepared in deionised water in PBS (phosphate buffer solution, at pH 7.41). 10^{-3} M solution of other biomolecules such as ascorbic acid (AA), glucose (Glu), uric acid (UA) and cholesterol were similarly prepared. The UV-Vis spectrum of RANH@MCM-48 in methanol was measured and the excitation wavelength for the fluorescence spectroscopic experiments was fixed at 280 nm. Fig. 6 shows the fluorescence spectra of RANH@MCM-48 in the presence of one equivalent of

DA, AA, UA, Glucose and Cholesterol. Fluorescence enhancement was observed only in case of DA while AA, UA, Glucose and Cholesterol had no significant effect on the fluorescence spectra of RANH@MCM-48. Fig. 7 shows the fluorescence spectra of RANH@MCM-48 at different added concentration of DA in aqueous solution. Fig. 7, inset shows the plot of fluorescence intensity *vs.* DA concentration which is linear. The linear range was found to be 0.5×10^{-5} M to 6×10^{-5} M. Since AA is the main interfering agent of DA detection in biological fluids and therefore we recorded fluorescence spectra of RANH@MCM-48 in the presence of AA (Fig. 8). From the figure it is clear that DA could enhance the fluorescence intensity of RANH@MCM-48 even in the presence of AA rather to a higher extent of about thirty times. Fig. 8, inset shows that the linear range for DA detection in the presence of AA is 0.5×10^{-5} M to 5×10^{-5} M. The limit of detection (LOD) for the sensing ability of RANH@MCM-48 towards DA were calculated as per reported method [45] and found to be 65nM and 51 nM respectively in absence and in presence of AA.

UV-Vis spectra of RANH@MCM-48 were recorded in methanol at different added concentration of DA (Fig. 9). It can be seen that the hump at 281 nm of RANH@MCM-48 becomes prominent with the increase in DA concentration. Inset of the figure shows the plot of fluorescence intensity as a function of DA concentration which is linear and the range is similar to that obtained from fluorescence data.

The reversibility of binding of DA to RANH@MCM-48 has been observed with respect to $EDTA^{2-}$ (Fig. 10). The fluorescence intensity of RANH@MCM-48 in the presence of one equivalent of DA was found to decrease with increase in added concentration of $EDTA^{2-}$. This clearly indicates that the interaction of RANH@MCM-48 with DA is reversible, which is a primary criteria for a good sensor.

Fig. 11 shows the effect of pH on fluorescence intensity of RANH@MCM-48 and RANH@MCM-48 in presence of DA in universal buffer solution. In case of RANH@MCM-48, the fluorescence intensity increases very little from pH 2.0 to 6.6, then increases marginally till pH 9.2 and decreases till pH 10.2 and remains almost unchanged. In case of RANH@MCM-48 in presence of DA, it was found that the fluorescence intensity remains almost constant in the range of pH 2.0 to 6.6 and suddenly it raises by nine times to attain maximum at pH 7.2. Then fluorescence intensity suddenly starts to drop when pH becomes 8.8 and becomes lowest at pH 9.2 which remains almost same till pH 12.0. Hence the fluorescence window is very narrow i.e. from 7.2 to 8.8 and is in the biological fluid range. Therefore, all the fluorescence measurements were taken at the pH value of 7.4 to avoid any fluorescence fluctuations.

Biological Applications

Detection of DA in artificial cerebrospinal fluid (ACF)

The ability of RANH@MCM-48 to determine DA in ACF was carried out. For this purpose, 5 mL solution of RANH@MCM-48 in PBS was spiked with 300 mL of ACF. The spiked RANH@MCM-48 solution was then titrated against different added concentration of DA by Fluorescence Spectroscopy. An enhancement of fluorescence intensity by about twenty times was observed with a linear intensity *vs.* DA concentration

plot in the range 0.5×10^{-5} M to 6.0×10^{-5} M (Fig. 12) which suggests the successful detection of DA in ACF medium. The LOD in synthetic ACF medium is calculated to be 27 nM.

Determination of DA in Bovine Serum Albumin (BSA)

The sensor RANH@MCM-48 was successfully applied for detection of DA in bovine serum albumin (BSA) in PBS (pH 7.4). Fig. 13 shows an enhancement of fluorescence intensity for RANH@MCM-48 in BSA medium by about nineteen times and the inset shows linear enhancement in intensity as a function of DA concentration in the range 0.5×10^{-5} M to 6.0×10^{-5} M. The LOD in BSA medium is calculated to be 22.5 nM.

Electrochemical sensing of DA by RANH@MCM-48

To study the electrochemical behavior of RANH@MCM-48 and its interaction with DA in the presence of AA, the cyclic voltammetry technique was used. A three electrode electrochemical cell consisting of modified platinum (Pt) electrode as working electrode, Ag-AgCl as reference electrode and Pt wire as an auxiliary electrode was used.

Fig. 14 shows the cyclic voltammogram of RANH@MCM-48/Pt in aqueous medium (PBS, pH=7.41) in the absence of DA (red line) and in the presence of DA (black line). In absence of DA one irreversible reduction peak at -0.497 V was observed which may be due to the electrochemical reduction of $[RAN]^+$ ion into neutral RAN free radical which subsequently breaks down as shown in scheme 2 [46]. In the presence of DA (black line) the cyclic voltammogram shows a redox couple with reduction peak at +0.036 V and oxidation peak at +0.228 V. The separation in peak potential (ΔE) was found to be 0.192 V and $E_{1/2}$ was calculated to be +0.132 V.

Fig. 15 shows that RANH@MCM-48/Pt electrode is capable of resolving the overlapping oxidation peaks of DA and AA at bare platinum electrode into two distinct oxidation peaks in the mixture of 0.5 mM DA and 1 mM AA. The peak for AA was observed at +0.503 V while the peak for DA was observed at +0.315 V. The separation between the oxidative peaks of AA and DA has been +0.188 V, hence the simultaneous detection of DA in the presence of AA is feasible at modified electrode. The oxidation currents for DA and AA were found to increase with the increase in their concentration simultaneously (Fig. 16). The plot of oxidation current for DA *vs.* its concentration in the presence of AA was linear (Inset, Fig. 16). Also, as the scan rate increases, the peak currents corresponding to DA and AA increases (Fig. 17).

The Limit of Detection (LOD) of DA in the presence of AA from cyclic voltammogram was calculated using the formula [47]: $3\sigma/K$, where σ = Standard Deviation, K= slope obtained from the plot of Anodic Current *vs.* concentration (Fig 16, inset). The LOD was calculated to be 77.5 nM.

Influence of other substances in the voltammetric detection of DA and AA

To study the influence of biologically important species that generally co-exist with DA in biological fluids, on the voltammetric detection of DA and AA, the cyclic voltammogram was recorded for DA and AA

mixture in presence of Na^+, K^+, Ca^{2+}, Fe^{2+}, Uric acid, Cholesterol and Glucose. It was found that the presence of these ions/compounds did not interfere with the simultaneous detection of DA and AA by the modified Pt electrode as shown in Fig. 19. The modified electrode has been employed to detect DA in PBS (pH 7.4) spiked with ACF and in BSA with LOD and linear range similar to those in PBS (pH 7.4).

Conclusion

The dye Rosaniline hydrochloride has been successfully encapsulated in MCM-48. This encapsulated MCM-48 can detect neurotransmitter dopamine by fluorescence “on” mode in phosphate buffer solution at pH 7.41 as well as in the artificial Cerebrospinalfluid and bovine serum albumin in the presence of ascorbic acid, glucose, cholesterol and uric acid. The linear range of detection is 0.5×10^{-5} M to 5.0×10^{-5} M with limits of detection in nano molar range. Platinum disc electrode modified with the dye encapsulated MCM-48 affects 0.188 V separation in oxidation potential of ascorbic acid and dopamine compared to overlapping oxidation potential at a bare platinum electrode. The linear range of detection for dopamine by voltammetry is 5×10^{-5} M to 50.0×10^{-5} M with limits of detection in nano molar range in presence of Na^+, K^+, Ca^{2+}, Fe^{2+}, ascorbic acid Uric acid, Cholesterol and Glucose in phosphate buffer solution at pH 7.41 as well as in artificial Cerebrospinalfluid and bovine serum albumin.

Declarations

Acknowledgement:

The authors thank SERB (Department of Science and Technology), New Delhi for financial support vide project (EMR/2016/001745) and FIST to the department.

Declarations: Funding statement Funding received from DST, New Delhi (EMR/2016/001745).

Data availability statement: Data sharing not applicable to this article as no datasets were generated or analysed during the current study.

Conflict of interest: There are no conflict to declare.

Ethics approval: Not applicable.

Consent to participate: Not applicable.

Consent for publication: Not applicable.

Author contribution: SK has done all the experiments works; DKD has done analysis of the results and written the paper.

References

1. Miller TS, Macpherson JV, Unwin PR (2015) Controlled functionalisation of single-walled carbon nanotube network electrodes for the enhanced voltammetric detection of dopamine. Phys Chem Chem Phys17:26394–26402. https://doi.org/10.1039/C5CP04905A
2. Thirumalraj B, Palanisamy S, Chen SM, Lou BS (2016) Preparation of highly stable fullerene C60 decorated graphene oxide nanocomposite and its sensitive electrochemical detection of dopamine in rat brain and pharmaceutical samples. J Colloid Interface Sci462:375–381. https://doi.org/10.1016/j.jcis.2015.10.009
3. Silva TR, Vieira ICA (2016) Biosensor based on gold nanoparticles stabilized in poly (allylamine hydrochloride) and decorated with laccase for determination of dopamine. Analyst141:216–224.https://doi.org/10.1039/C5AN01784J
4. Zhang X, Chen X, Kai S, Wang HY, Yang J, Wu FG, Chen Z (2015) Highly Sensitive and Selective Detection of Dopamine Using One-Pot Synthesized Highly Photoluminescent Silicon Nanoparticles. Anal Chem 87:3360. https://doi.org/10.1021/ac504520g
5. Oak JN, Oldenhof J, Van Tol HH (2000) The dopamine D 4 receptor: one decade of research. EurJ Pharmacol405:303–327. https://doi.org/10.1016/s0014-2999(00)00562-8
6. Adekunle AS, Agboola BO, Pillay J, Ozoemena KI (2010) Electrocatalytic detection of dopamine at single-walled carbon nanotubes–iron (III) oxide nanoparticles platform. Sens ActuatorB-Chem 148:93–102. https://doi.org./10.1016/j.snb.2010.03.088
7. Liu L, Li S, Liu L, DengD, Xia N (2012) Simple, sensitive and selective detection of dopamine using dithiobis(succinimidylpropionate)-modified gold nanoparticles as colorimetric probes. Analyst 137:3794-3799.https://doi.org/10.1039/C2AN35734H
8. Li N, Gao J, Liu B, Yu Y, Cui H, Mao L, Lin Y (2009) Determination of monoamine neurotransmitters and their metabolites in a mouse brain microdialysate by coupling high-performance liquid chromatography with gold nanoparticle-initiated chemiluminescence. Anal Chim Acta 645:48–55. https://doi.org/10.1016/j.aca.2009.04.050
9. Liu JM, Cui ML, Jiang SL, Wang XX, Lin LP, Jiao L, Zhang LH, Zheng ZY (2013) BSA-protected gold nanoclusters as fluorescent sensor for selective and sensitive detection of pyrophosphate. Anal Methods 5:3942–3947. https://doi.org/10.1039/C3AY00054K
10. Kim Y, Bong S, Kang Y, Yang Y, Mahajan RK, Kim JS, Kim H (2010) Electrochemical detection of dopamine in the presence of ascorbic acid using graphene modified electrodes. Biosens Bioelectron 25:2366–2369. https://doi.org/ 10.1016/j.bios.2010.02.031
11. Wang A, Feng J, Dong W, Lu Y, Li Z, Riekkola ML (2010) Spermine-graft-dextran non-covalent copolymer as coating material in separation of basic proteins and neurotransmitters by capillary electrophoresis. J Chromatogr A 1217:5130 –5136. https://doi.org/10.1016/j.chroma.2010.06.019
12. Su H, Sun B, Chen L, Xu Z, Ai S (2012) Colorimetric sensing of dopamine based on the aggregation of gold nanoparticles induced by copper ions. Anal Methods 4: 3981-3986. https://doi.org/10.1039/C2AY25794G

13. Zhang L, Teshima N, Hasebe T, Kurihra M, Kawashima T (1999) Flow-injection determination of trace amounts of dopamine by chemiluminescence detection. Talanta 50:677-683. https://doi.org/10.1016/s0039-9140(99)00164-2
14. Mu Q, Xu H, Li Y, Ma S, Zhong X (2014) Adenosine capped QDs based fluorescent sensor for detection of deopami8ne with high selectivity and sensitivity. Analyst 139:93-98. https://doi.org/10.1039/C3AN01592K
15. Liu L, Du J, Li S, Yuan B, Han H, Jing M, Xia N (2013) Amplified voltammetric detection of dopamine using ferrocene-capped gold nanoparticle/streptavidin conjugates. Biosens Bioelectron 41:730–735. https://doi.org/10.1016/j.bios.2012.09.061
16. Alfredsson V, Anderson MW (1996) Structure of MCM-48 revealed by transmission electron microscopy. Chem Mater 8:1141–1146. https://doi.org/10.1021/cm950568k
17. Schumacher K, Grun M, Unger KK (1999) Novel synthesis of spherical MCM-48. Micropor Mesopor Mat 27:201–206. https://doi.org/10.1016/S1387-1811(98)00254-6
18. Kim JM, Kim SK, Ryoo R (1998) Synthesis of MCM-48 single crystals. Chem Commun 2:259–260. https://doi.org/10.1039/A707677K
19. Bandyopadhyay M, Birkner A, van den Berg MWE, Klementiev KV, Schmidt W, Grunert W, Gies H (2005) Synthesis and Characterization of Mesoporous MCM-48 Containing TiO_2 Nanoparticles. Chem Mater 17:3820-3829.
20. Liu JW, Stace-Naughton A, Jiang XM, Brinker CJ (2009) Porous Nanoparticle Supported Lipid Bilayers (Protocells) as Delivery Vehicles. J Am Chem Soc 131:1354-1355. https://doi.org/10.1021/ja808018y
21. Yang P, Yang P, Teng X, Lin J, Huang L (2011) A novel luminescent mesoporous silica/apatite composite for controlled drug release. J Mater Chem 21:5505–5510. https://doi.org/10.1039/C0JM03878D
22. Aghaei H, Nourbakhsh AA, Karbasi S, Javadkalbasi R, Rafienia M, Nourbakhsh N, Bonakdar S, Mackenzie KJD (2014) Investigation on bioactivity and cytotoxicity of mesoporous nano-composite MCM-48/hydroxyapatite for ibuprofen drug delivery. Ceram. Int. 40:7355–7362. https://doi.org/10.1016/j.ceramint.2013.12.079
23. Zhoua Y, Quana G, Wub Q, Zhangc X, Niua B, Wua B, Huanga Y, Pan X, Wua C (2018) Mesoporous silica nanoparticles for drug and gene delivery Acta Pharmaceutica Sinica B 8:165-177. https://doi.org/10.1016/j.apsb.2018.01.007
24. Romero A, Nieto-Marquez A, Alonso E (2017) Bimetallic Ru:Ni/MCM-48 catalysts for the effective hydrogenation of d-glucose into sorbitol. Appl Catal A-Gen 529:49-59. https://doi.org/10.1016/j.apcata.2016.10.018
25. Li S, Tang Y, Chen W, Hu Z, Li X, Li L (2017) Heterogeneous catalytic ozonation of clofibric acid using Ce/MCM-48: Preparation, reaction mechanism, comparison with Ce/MCM-41. J Colloid Interface Sci 504:238-246. https://doi.org/10.1016/j.jcis.2017.05.042

26. Kim S, Ida J, Guliants VV, Lin JYS (2005) Tailoring Pore Properties of MCM-48 Silica for Selective Adsorption of CO_2. J Phys Chem B 109:6287-6293. https://doi.org/10.1021/jp045634x

27. Jang HT, Park YK, Ko YS, Lee JY, Margandan B (2009) Highly siliceous MCM-48 from rice husk ash for CO_2 adsorption. Int J Greenh 3:545-549. https://doi.org/10.1016/j.ijggc.2009.02.008

28. Macario A, A Katovic, G Giordano, F Iucolano, D Caputo (2005) Synthesis of mesoporous materials for carbon dioxide sequestrationMicropor Mesopor Mat 81:139-147.http://dx.doi.org/10.1016/j.micromeso.2005.02.002

29. Huang HY, Yang RT, Chinn D, Munson CL (2003) Amine-Grafted MCM-48 and Silica Xerogel as Superior Sorbents for Acidic Gas Removal from Natural Gas. Ind Eng Chem Res 42:2427-2433.https://doi.org/10.1021/ie020440u

30. Anbia M, Kargosha K, Khoshbooei S (2015) Heavy metal ions removal from aqueous media by modified magnetic mesoporous silica MCM-48. Chem Eng Res Des 93:779-788. https://doi.org/10.1016/j.cherd.2014.07.018

31. Zou Q, Zou L, Tian H (2011) Detection and adsorption of Hg^{2+} by new mesoporous silica and membrane material grafted with a chemodosimeter. J Mater Chem 21:14441. https://doi.org/10.1039/C1JM11704A

32. Yu H, Jia Y, Wu R, Chen X, Chan TW (2019) Determination of fluoroquinolones in food samples by magnetic solid-phase extraction based on a magnetic molecular sieve nanocomposite prior to high-performance liquid chromatography and tandem mass spectrometry. Anal Bioanal Chem 411:2817-2826. https://doi.org/10.1007/s00216-019-01726-0

33. Yousefi A, Babaei A (2018) A new sensor based on glassy carbon electrode modified with Fe_3O_4@MCM-48-SO_3H/multi-wall carbon nanotubes composite for simultaneous determination of norepinephrine and tyrosine in the presence of ascorbic acid. Ionics 25:2845–2856. https://doi.org/10.1007/s11581-018-2815-9

34. Yousefi A, Babaei A, Afrasiabi M (2019) Fe_3O_4@MCM-48-SO_3H/ Multi-Wall Carbon Nanotubes Composite Modified Glassy Carbon Electrode: an Efficient Sensor for Sensitive and Selective Simultaneous Determination of Serotonin and Sertraline in the presence of Uric Acid. Anal Bioanal Electrochem 11:1-18.

35. Sareen D, Kaur P, Singh K (2014) Strategies in detection of metal ions using dyes. Coord Chem Rev 265:125-154. https://doi.org/10.1016/j.ccr.2014.01.015

36. O'Neil C, Hawkes FR, Hawkes DL, Lourenco ND, Pinheiro HM, Delee W (1999) Colour in textile effluents – sources, measurement, discharge consents and simulation: a review. J Chem Technol Biotechnol 74:1009-1018. https://doi.org/10.1002/(SICI)1097-4660(199911)74:11<1009::AID-JCTB153>3.0.CO;2-N

37. Haloi, S., Goswami, P., Das, D.K., 2013.Differentiating response of 2,7 dichlorofluorescein intercalated CTAB modified Na-MMT clay matrix towards dopamine and ascorbic acid investigated by electronic,

fluorescence spectroscopy and electrochemistry. J Applied Clay Science 77-78, 79-82. https://doi.org/10.1016/j.clay.2013.01.017

38. Jianga Y, Abukhadrab MR, Refayc NM, Sharafe MF, El-Meligyf MA, Awwad EM (2020) Synthesis of chitosan/MCM-48 and β-cyclodextrin/MCM-48 composites as bio-adsorbents for environmental removal of Cd^{2+} ions, kinetic and equilibrium studies. React Funct Polym 154:104675.https://doi.org/10.1016/j.reactfunctpolym.2020.104675
39. Fathy M, Selim H, Shahawy AEL (2020) Chitosan/MCM-48 nanocomposite as a potential adsorbent for removing phenol from aqueous solution. RSC Adv 10:23417. https://doi.org/10.1039/D0RA02960B
40. Fayed TA, El-Nahass MN, El-Daly H, Shokry AA (2019) Development of nanomaterial chemosensors for toxic metal ion sensing. Appl Organometal Chem 33:4868. https://doi.org/10.1002/aoc.4868
41. Abolhasani J, Behbahani M (2015) Application of 1-(2-pyridylazo)-2-naphthol-modified nanoporous silica as a technique in simultaneous trace monitoring and removal of toxic heavy metals in food and water samples. Environ Monit Assess 187:4176. https://doi.org/10.1007/s10661-014-4176-9
42. Zablocka I, Wysocka-Zolopa M, Winkler K (2018) Electrochemical Detection of Dopamine at a Gold Electrode Modified with a Polypyrrole–Mesoporous Silica Molecular Sieves (MCM-48) Film. Int J Mol Sci 20:111. https://doi.org/10.3390/ijms20010111
43. De Toledo RA, Santos MC, Cavalheiro ETG (2005) Determination of dopamine in synthetic cerebrospinal fluid by SWV with graphite-polyurethane composite electrode. Anal Bioanal Chem 381:1161-1166. https://doi.org/10.1007/s00216-005-3066-y
44. Rajbongshi, J., Das, D.K., Mazumdar, S., 2010. Direct electrochemistry of dinuclear CuA fragment from cytochrome oxidase of Thermus thermophilus at surfactant modified glassy carbon electrode. Electrochim Acta 55, 4174-4179. https://doi.org/10.1016/j.electacta.2010.02.045
45. Lai X, Wang R, LiJ, Qiu G, Liu JB (2019) A cascade reaction-based switch-on fluorescent sensor for Ce(IV) ions in real samples. RSC Adv 9: 22053–22056. https://doi.org/10.1039/c9ra03776d
46. Iyum J F, Peters A O, Babutunde O A, (2002) Kinetics of reduction of triaminotolyldiphenylmethane chloride (rosaniline hydrochloride) by hydroxide ions in aqueous medium. Indian J Chem, 41A:967-969.
47. Hegde RN, Swamy BES, Shetti NP, Nandibewoor ST (2009) Electro-oxidation and determination of gabapentin at gold electrode. J Electroanal Chem 635:51–57. https://doi.org/10.1016/j.jelechem.2009.08.004

Figures

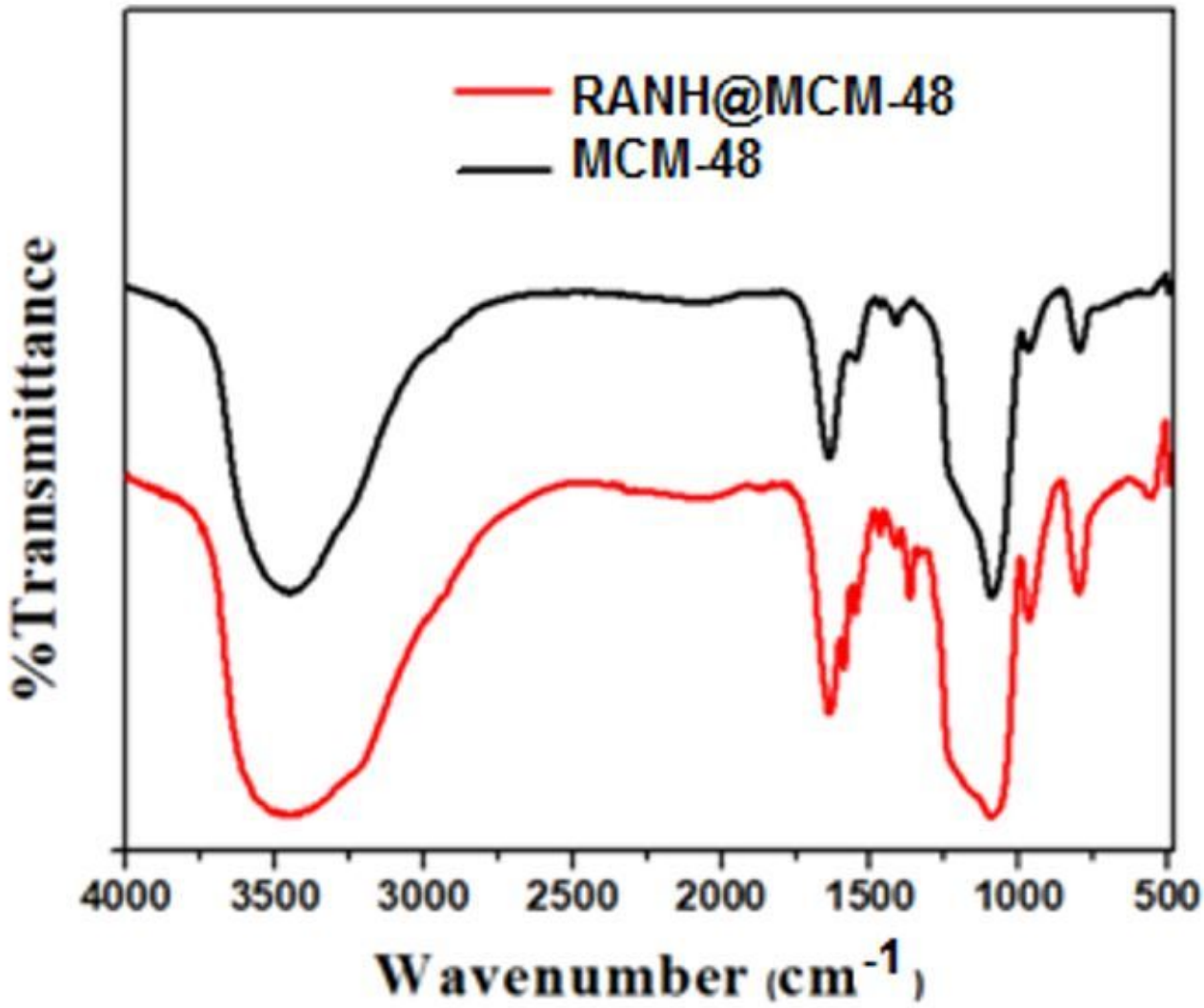

Figure 1

FTIR spectra of MCM-48 and RANH@MCM-48 as KBr pallet.

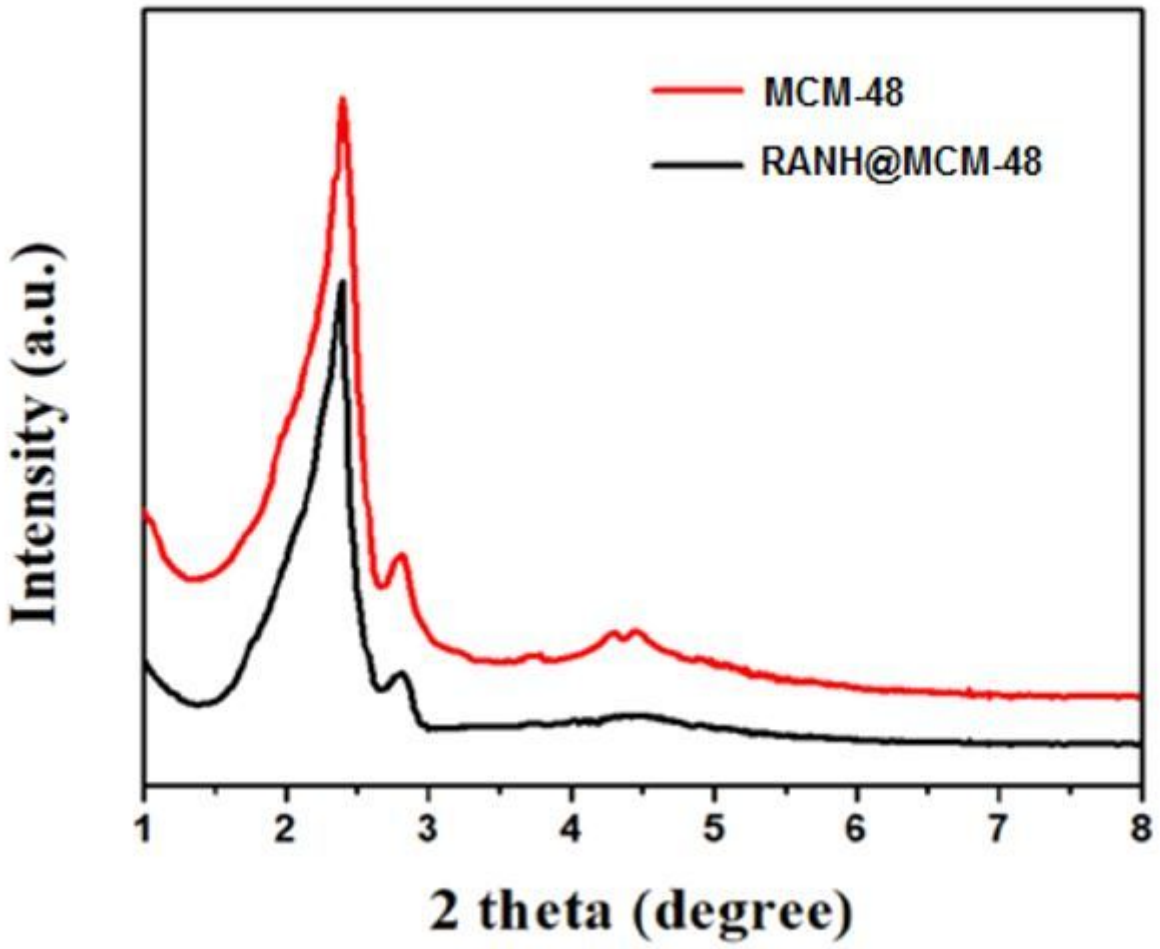

Figure 2

Low angle PXRD spectra of MCM-48 (red line) and RANH@MCM-48 (black line).

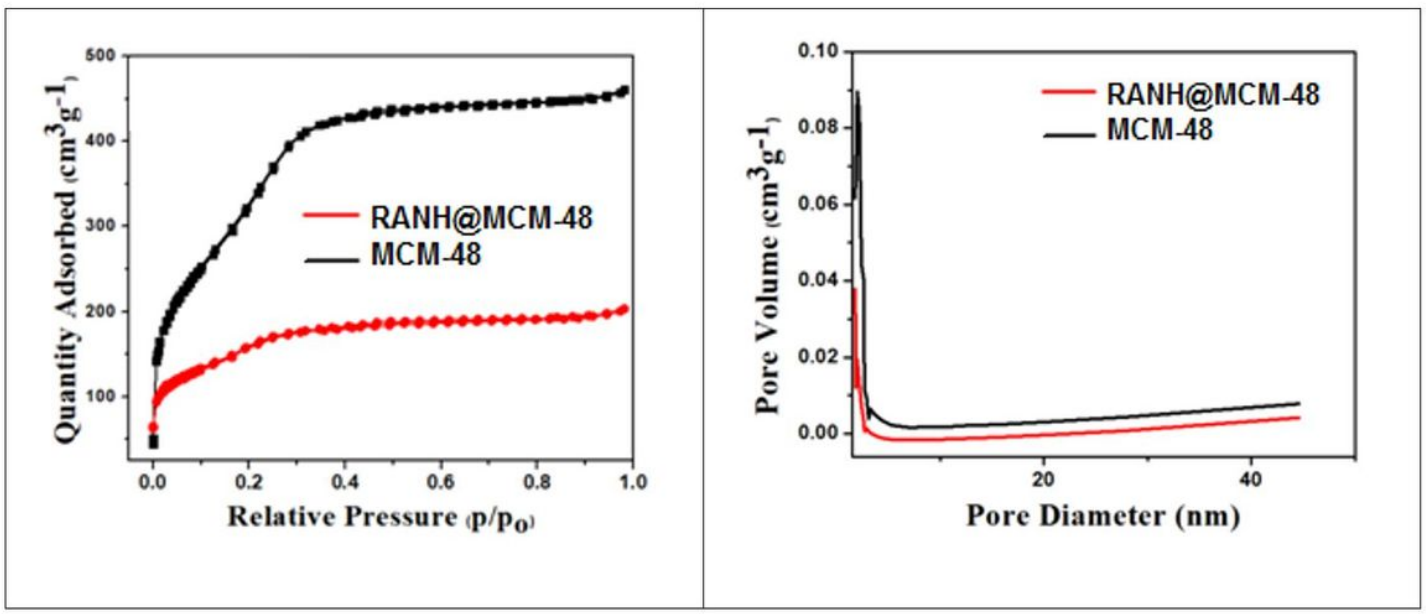

Figure 3

a) N2 adsorption-desorption isotherm of MCM-48 and RANH@MCM-48, b) Pore size distribution of MCM-48 and RANH@MCM-48.

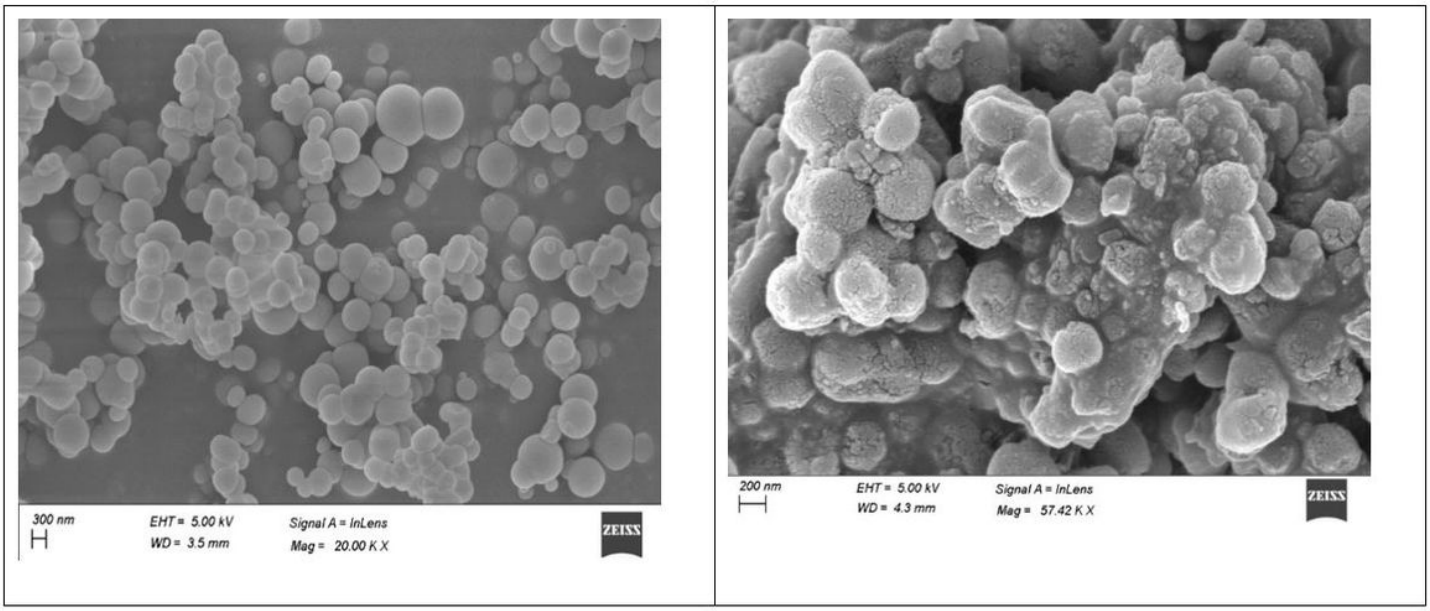

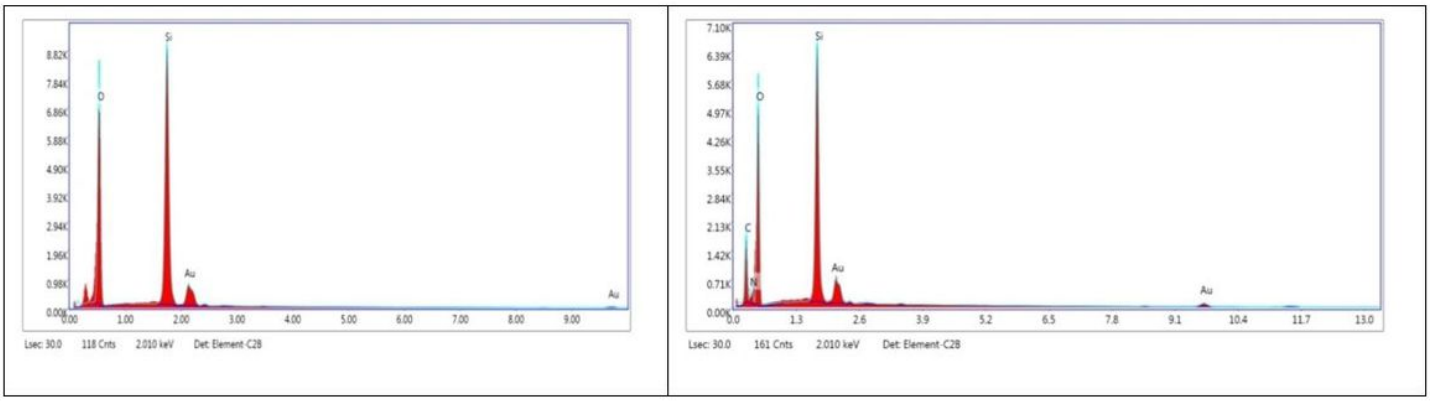

Figure 4

a) SEM image of MCM-48, b) SEM image of RANH@MCM-48, c) EDX spectra of MCM-48, d) EDX spectra of RANH@MCM-48.

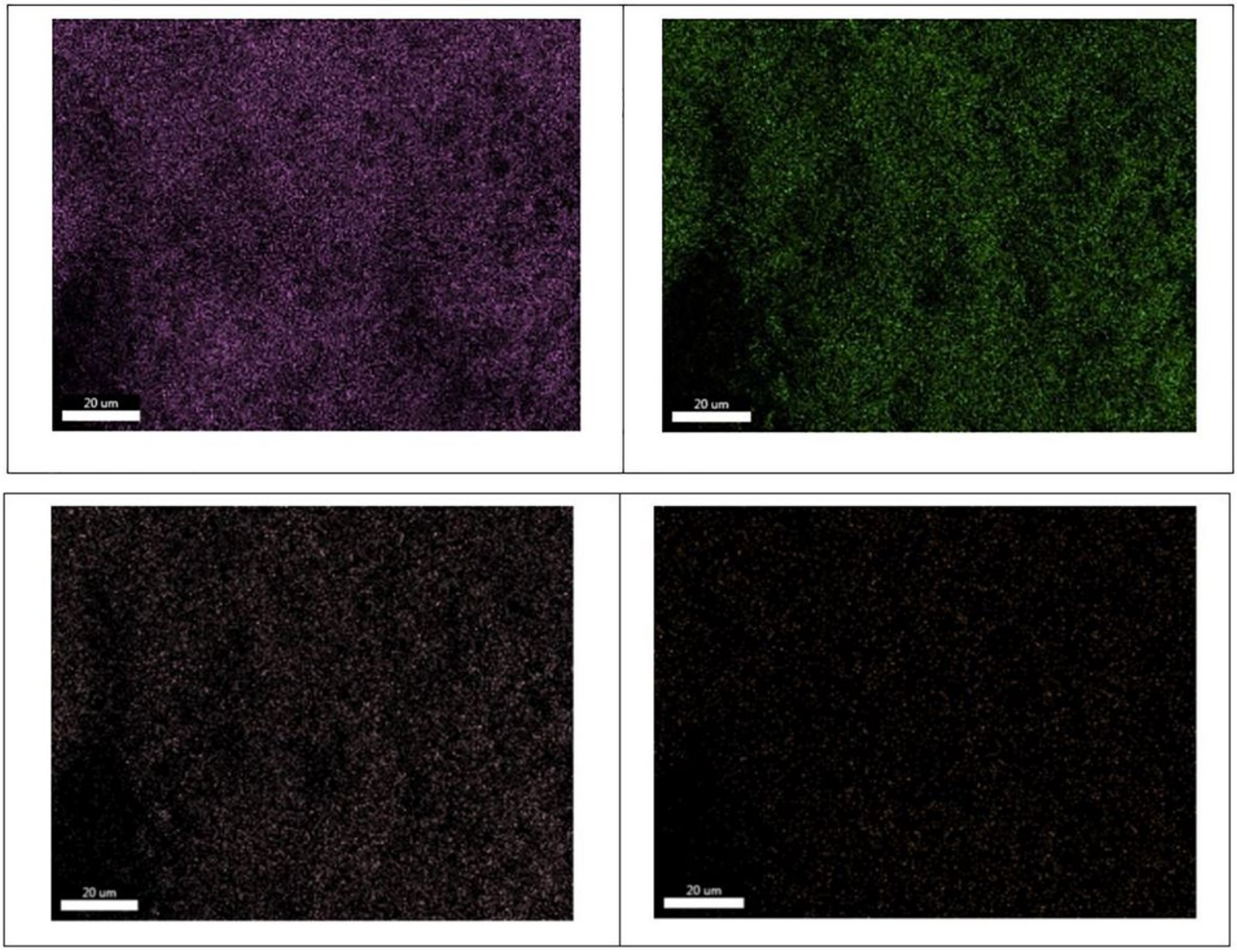

Figure 5

EDX elemental mapping of O, Si, C and N in RANH@MCM-48.

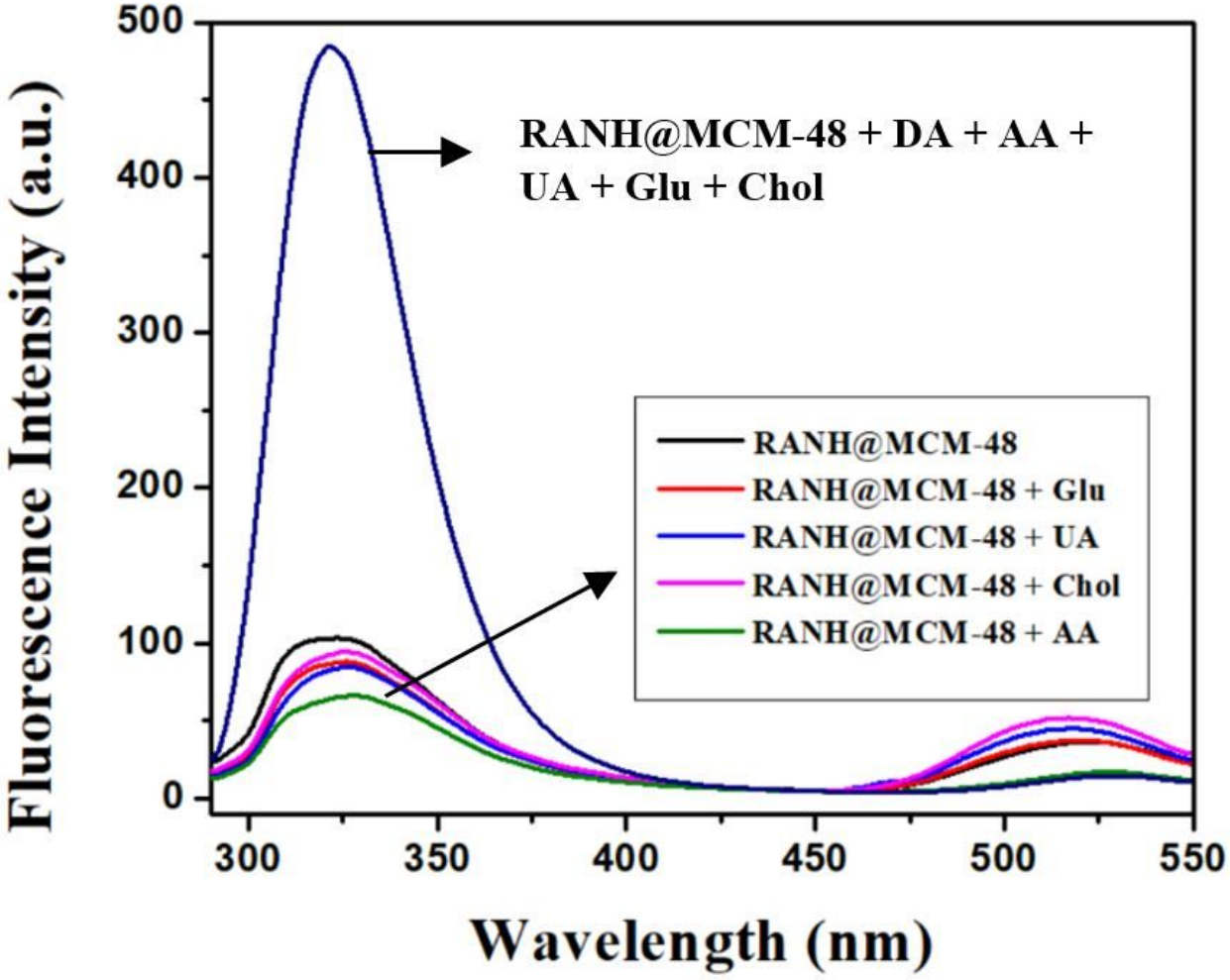

Figure 6

Fluorescence spectra of RANH@MCM-48 in presence of Glucose, UA, Cholesterol, AA and DA (in presence of all these bio-molecules) in methanol.

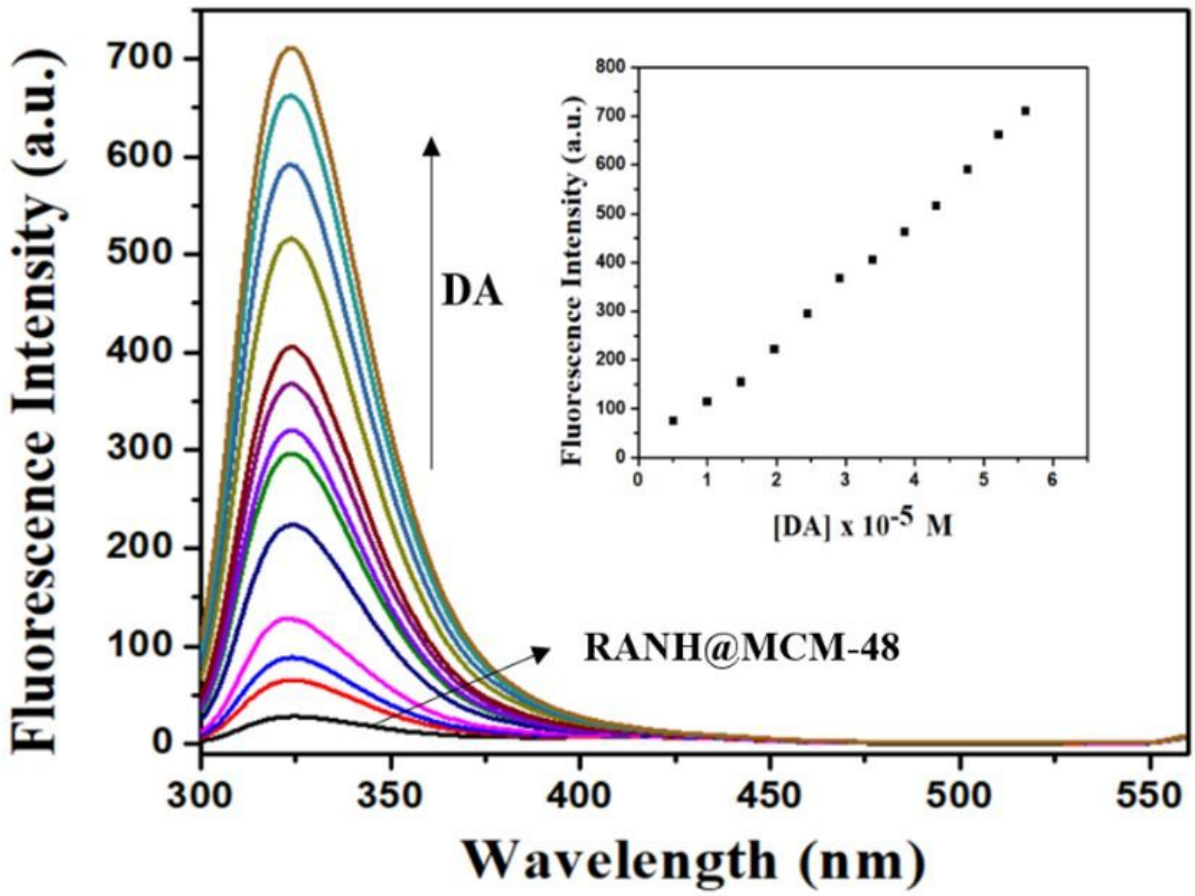

Figure 7

Fluorescence spectra of RANH@MCM-48 at different added concentration of DA in aqueous solution (pH=7.41, λex=280 nm, λmax= 326.2 nm). Inset: Plot of fluorescence intensity as a function of different concentration of DA.

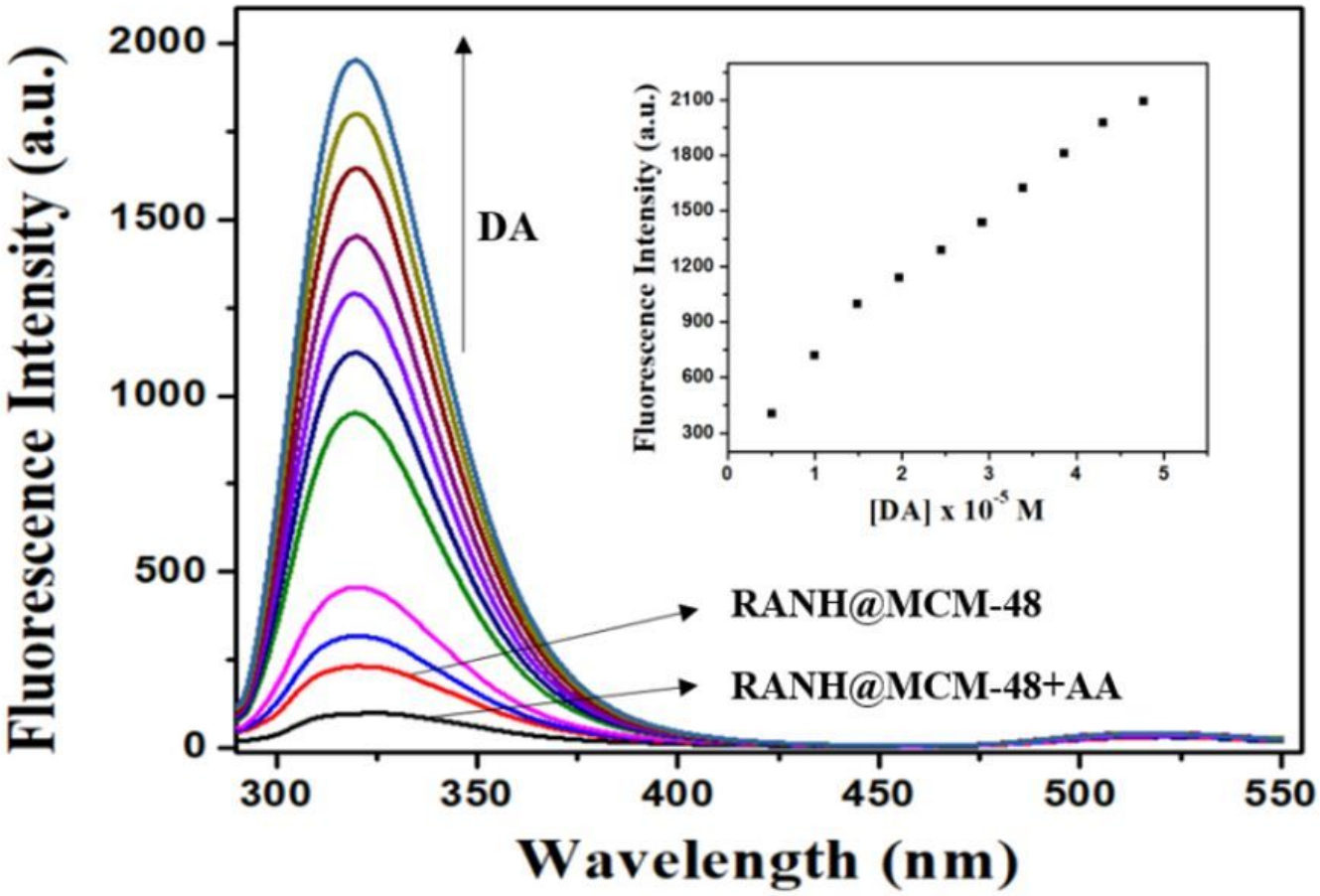

Figure 8

Fluorescence spectra of RANH@MCM-48 at different added concentration of DA in PBS in presence of AA (pH=7.41, λex=280 nm, λmax= 326.6 nm). Inset: plot of fluorescence intensity as a function of DA concentration in presence of AA.

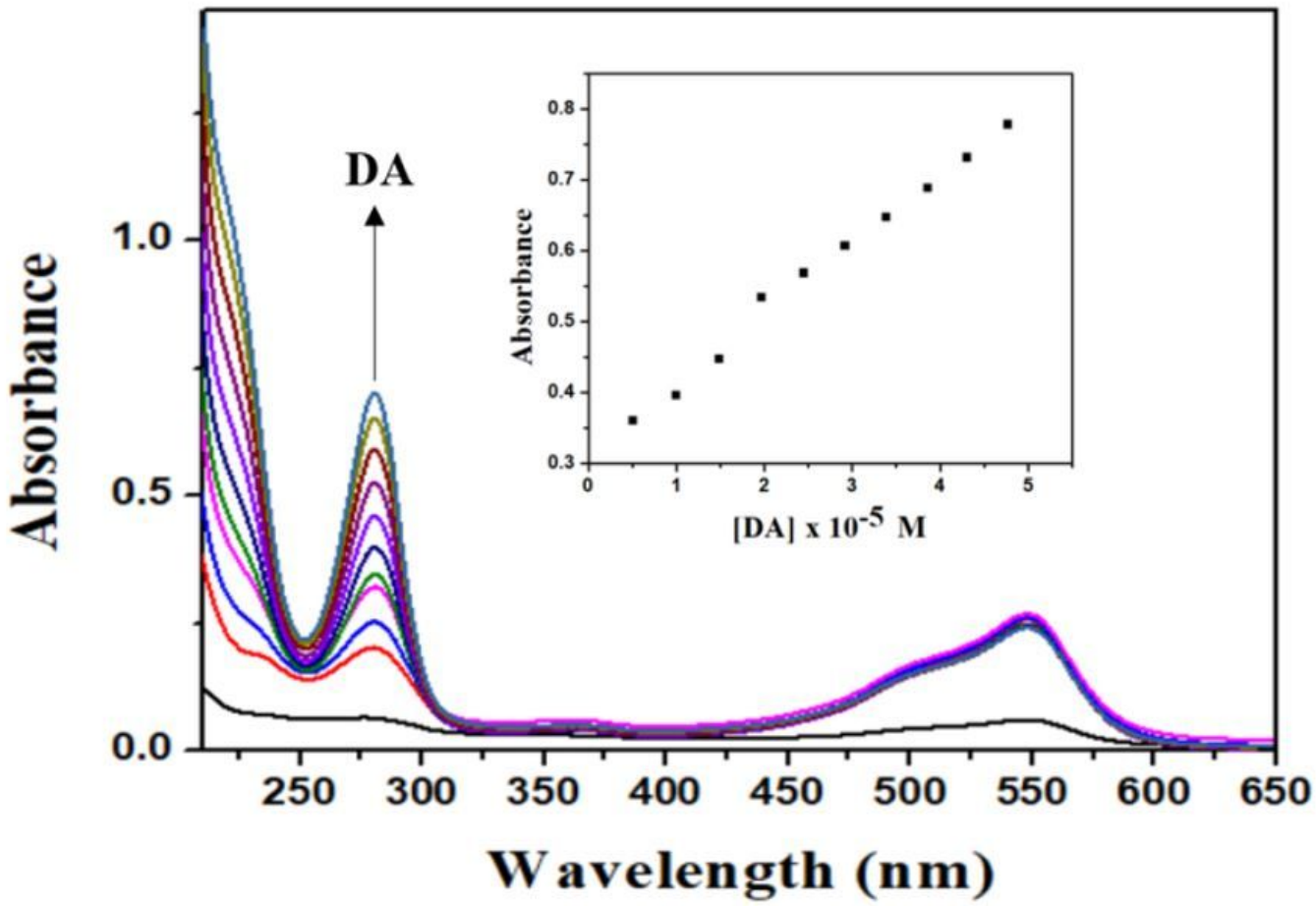

Figure 9

UV-Vis spectra of RANH@MCM-48 with different added concentration of DA. Inset: Plot of absorbance as a function of DA concentration.

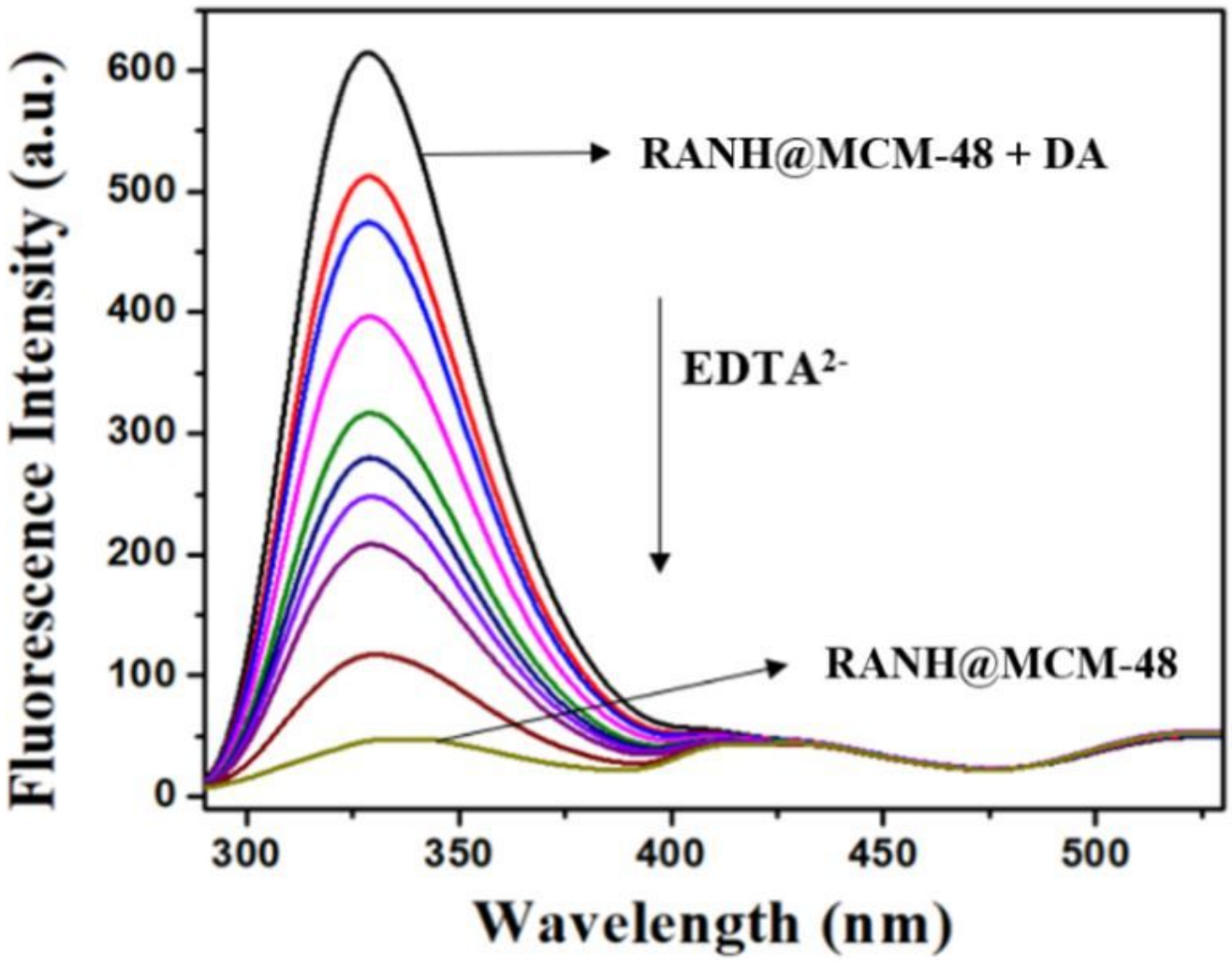

Figure 10

Fluorescence spectra of RANH@MCM-48:DA at different added concentration of EDTA2-.

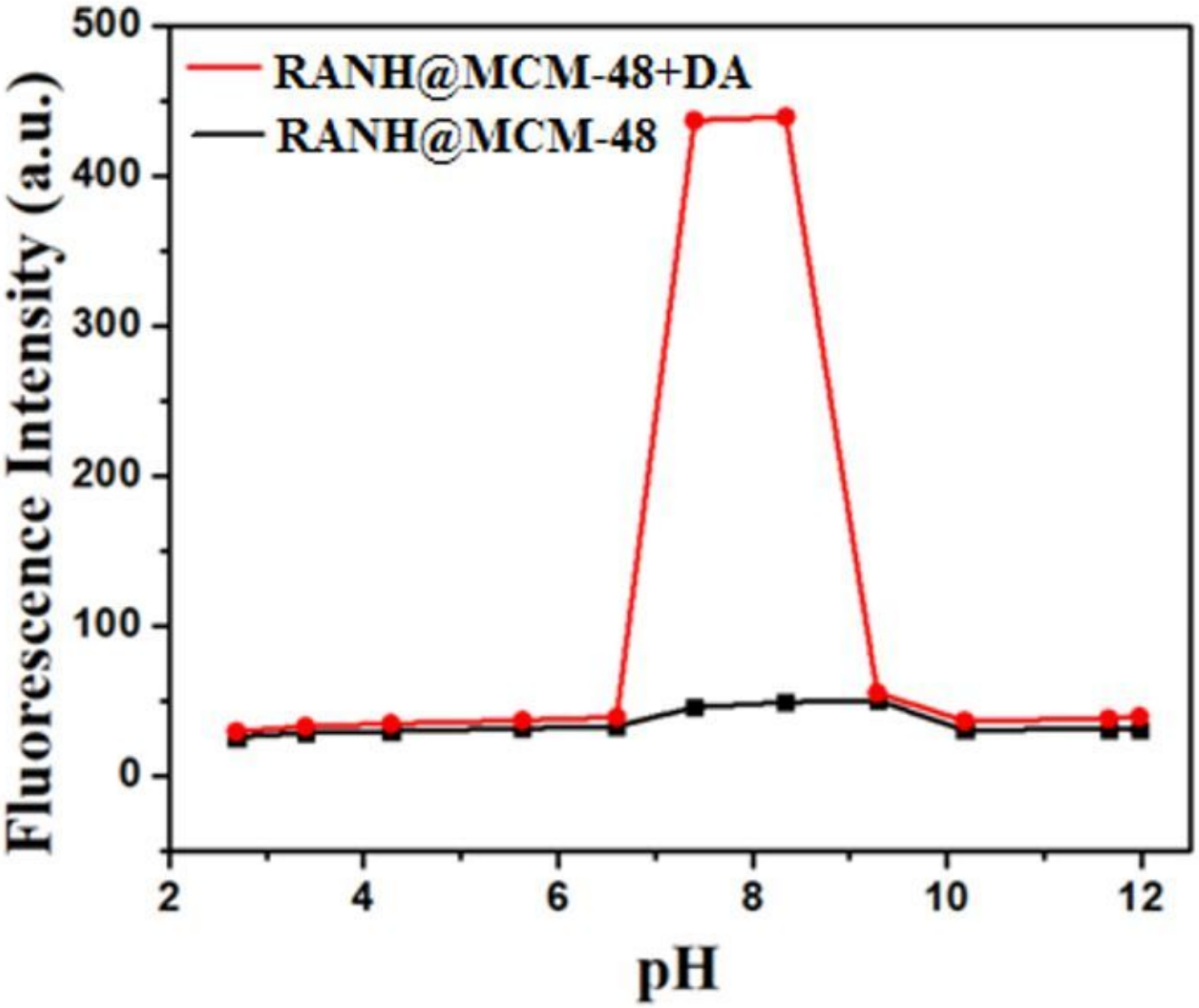

Figure 11

Effect of pH on the fluorescence intensity of RANH@MCM-48 and RANH@MCM-48+DA universal buffer solution

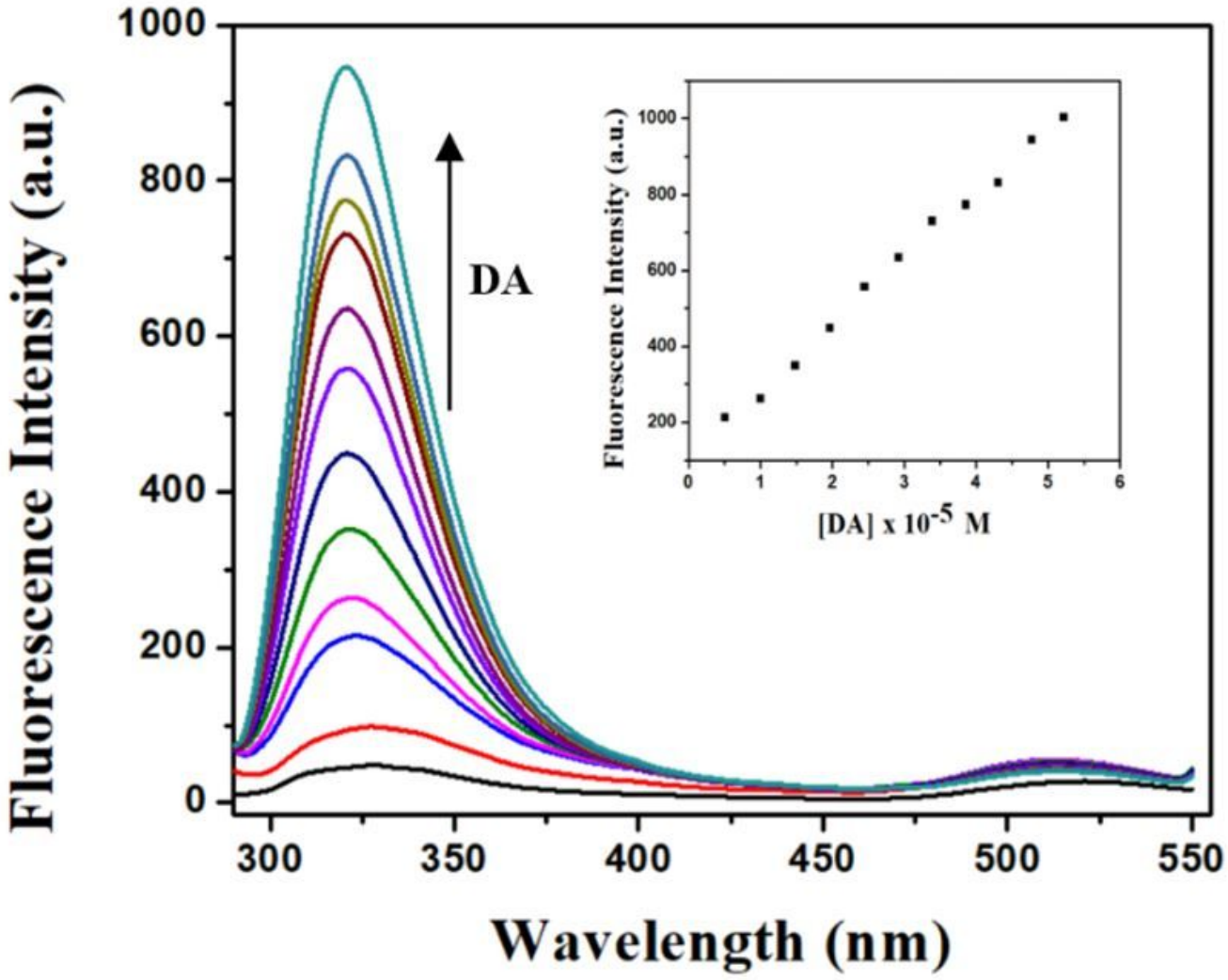

Figure 12

Fluorescence spectra of RANH@MCM-48 at different added concentration of DA in PBS (pH 7.41) spiked with ACF. Inset: Plot of fluorescence intensity vs. DA concentration.

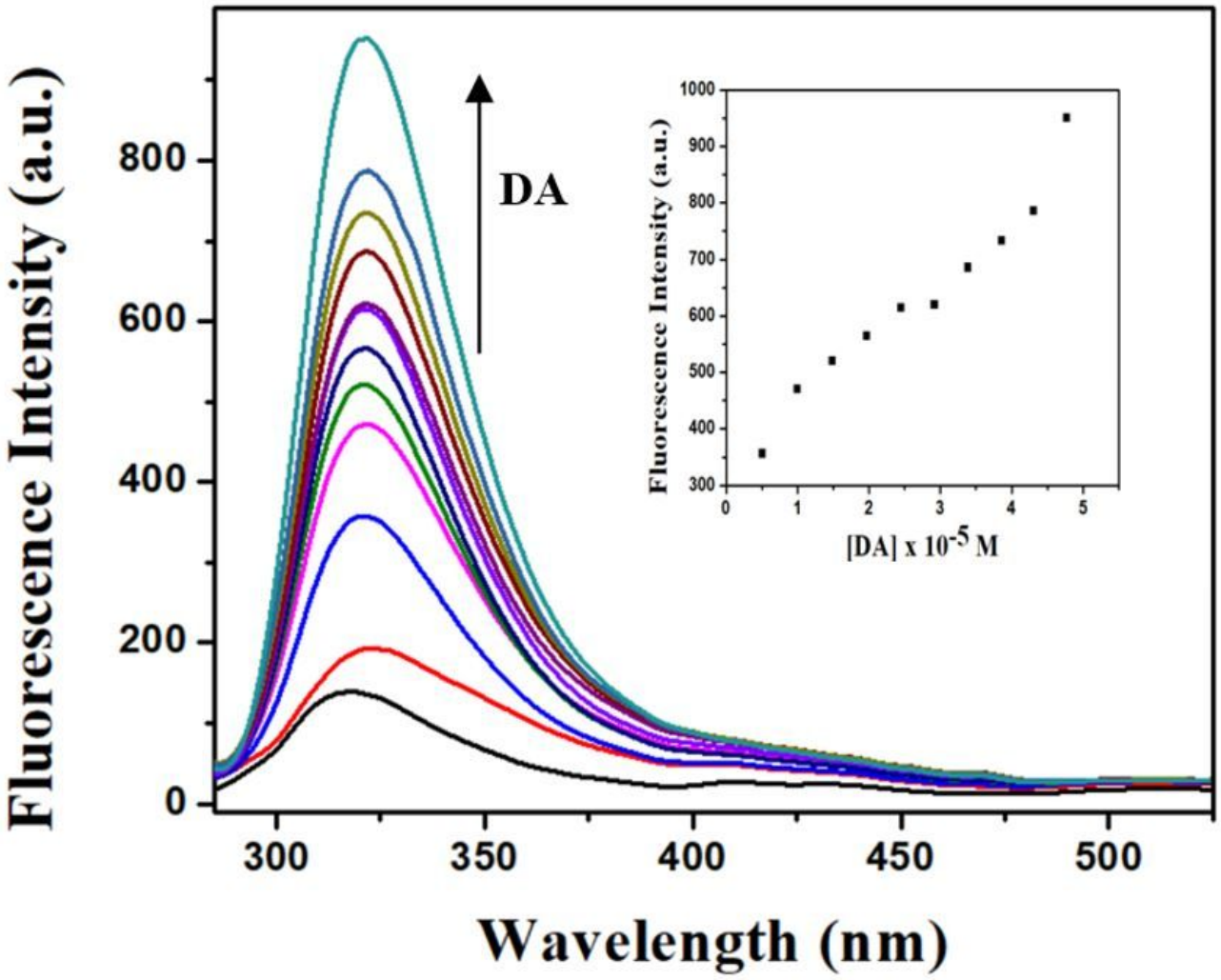

Figure 13

13Fluorescence spectra of RANH@MCM-48 at different added concentration of DA in BSA medium (PBS, pH 7.41). Inset: Plot of fluorescence intensity vs. DA concentration.

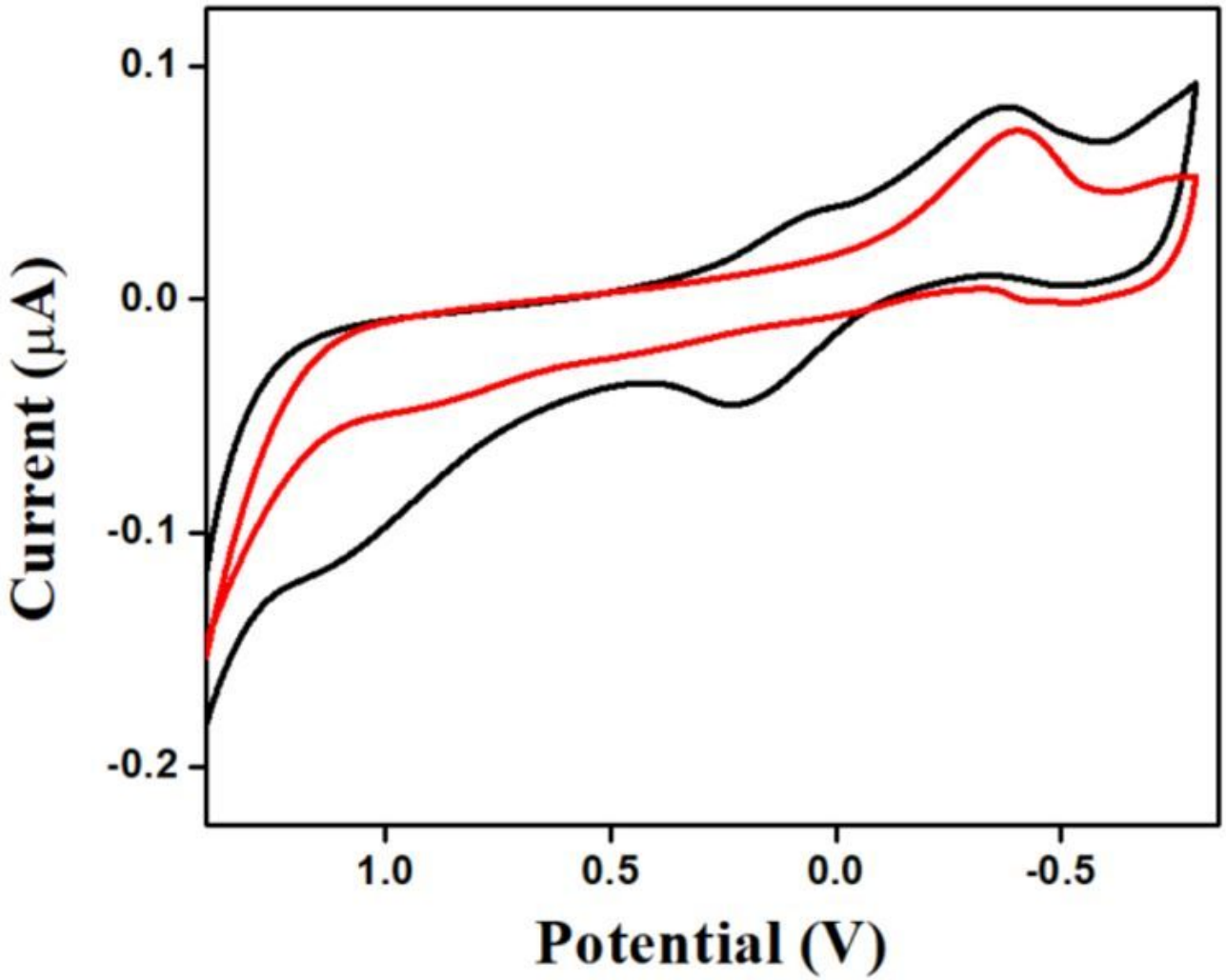

Figure 14

Cyclic Voltammogram of RANH@MCM-48/Pt electrode in PBS (pH=7.41) in absence (red line) of and presence of 1mM DA (black line). (RE: Ag-AgCl, SE: 0.1 M $NaNO_3$).

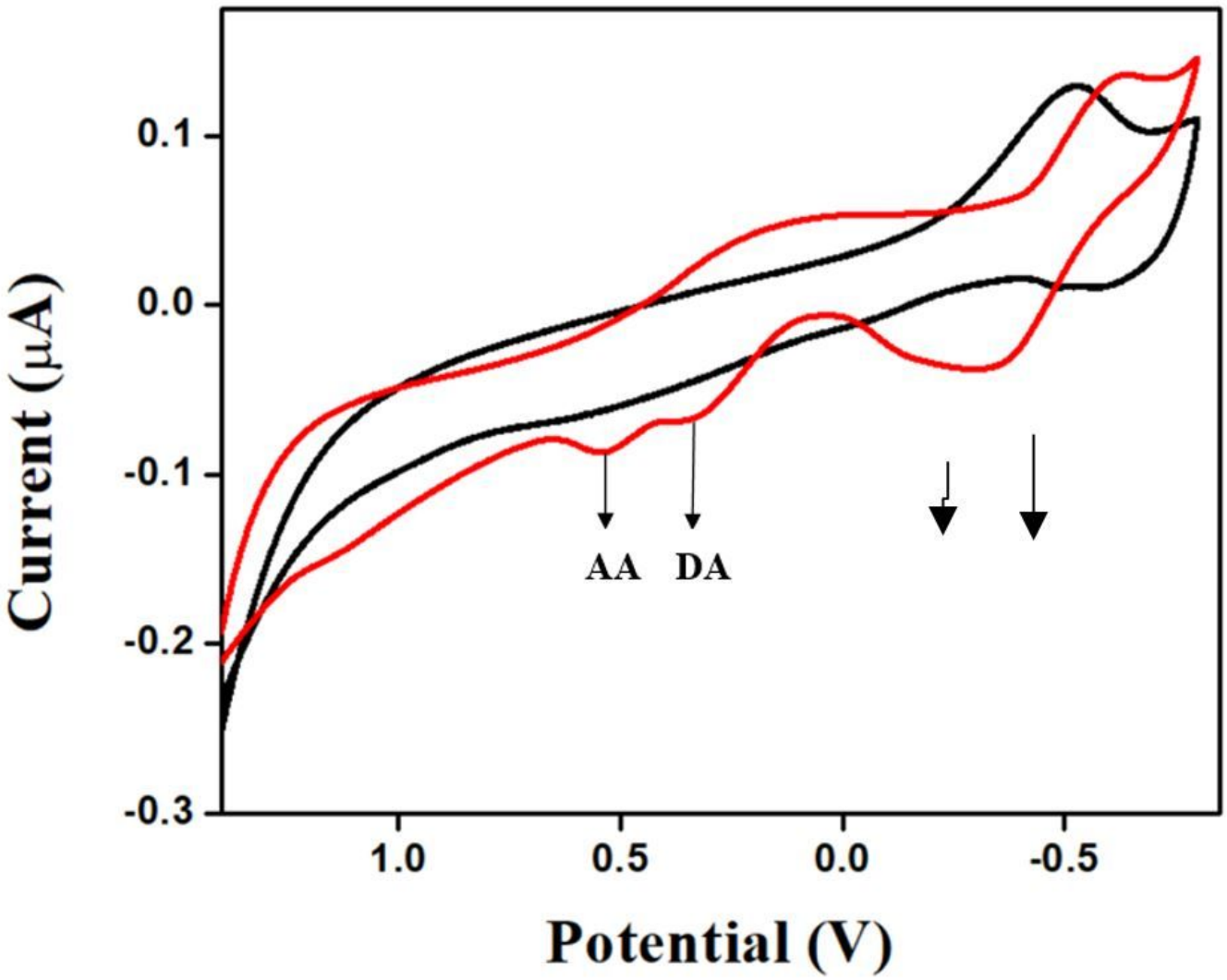

Figure 15

Cyclic Voltammogram at RANH@MCM-48/Pt in PBS containing 1mM AA and 0.5 mM DA (red line) in PBS (pH 7.41). (RE: Ag-AgCl, SE: 0.1 M NaNO3).

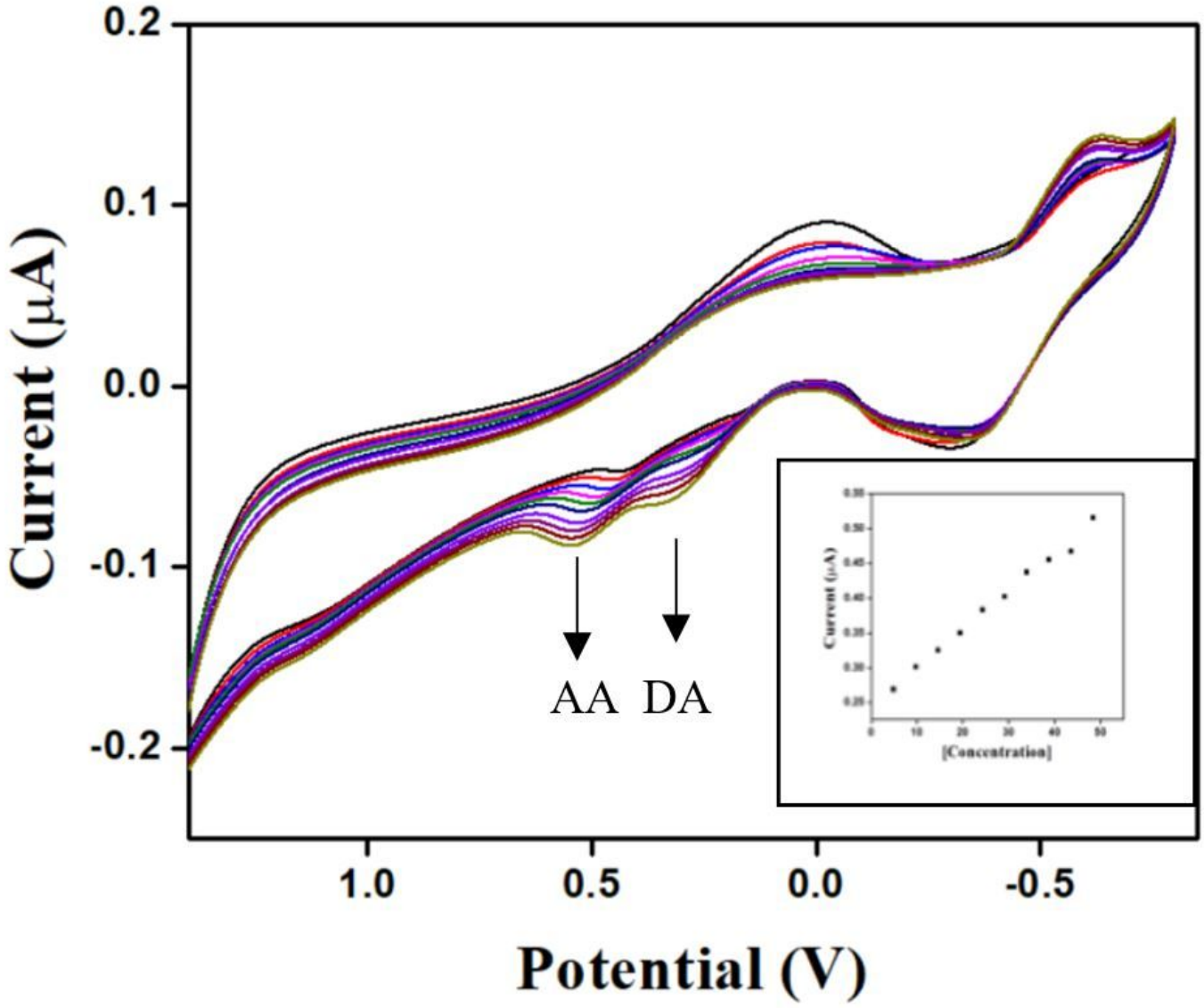

Figure 16

Cyclic Voltammogram of RANH@MCM-48/Pt electrode at different added concentration of DA and AA in PBS (pH 7.4). Inset: Plot of oxidation current for DA in presence of AA. (RE: Ag-AgCl, SE: 0.1 M NaNO3)

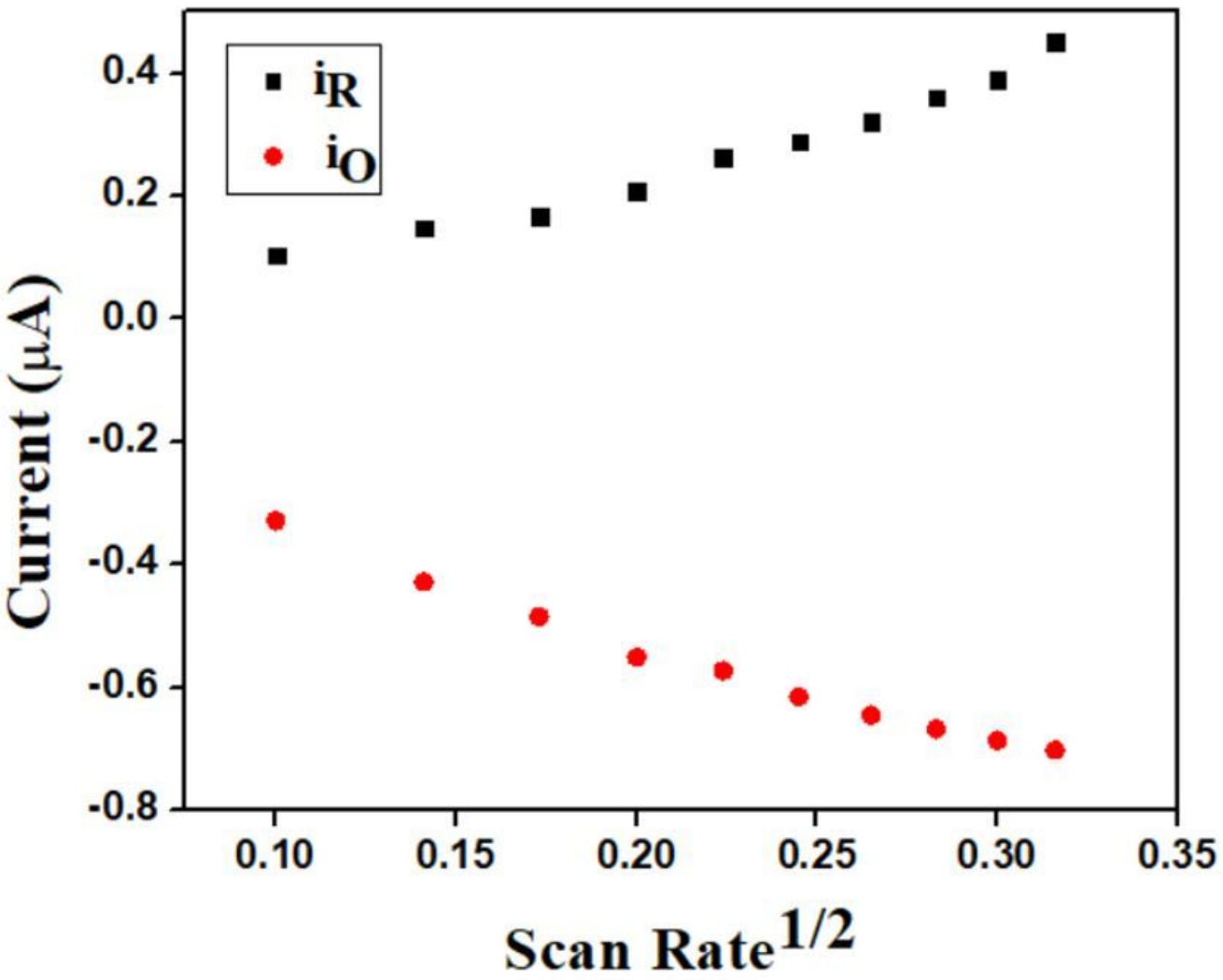

Figure 17

Linear plot of Scan Rate1/2 vs Current of 1mM AA and 0.5 mM DA.

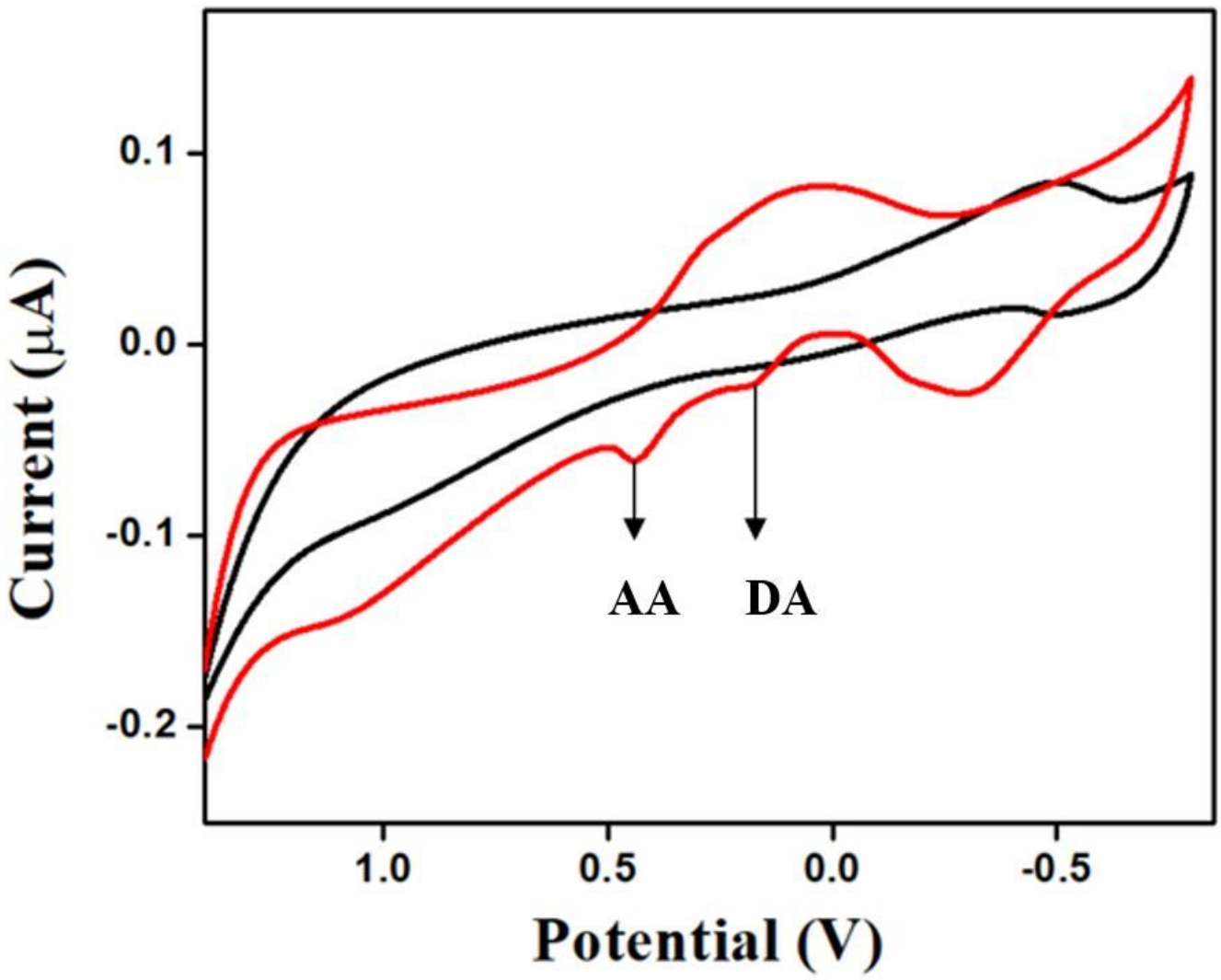

Figure 18

Cyclic Voltammogram of 0.5 mM DA and 1 mM AA in presence of Na+, K+, Ca2+, Fe2+, Uric acid, Cholesterol and Glucose at RANH@MCM-48/Pt electrode in aqueous medium. (RE: Ag-AgCl , 0.1 M NaNO3).

Supplementary Files

This is a list of supplementary files associated with this preprint. Click to download.

- scheme1.jpg
- scheme2.jpg